# Thermal Dynamics Modeling of a 3D Wind Sensor Based on Hot Thin Film Anemometry

Maria-Teresa Atienza*, Lukasz Kowalski, Sergi Gorreta, Vicente Jiménez, Manuel Domínguez-Pumar

*Micro and Nano Technologies Group, Electronic Engineering Department. Universitat Politècnica de Catalunya, Jordi Girona 1-3, 08034 Barcelona, Spain*

**Abstract**

The objective of this paper is to obtain time-varying models of the thermal dynamics of a 3D hot thin film anemometer for Mars atmosphere. To this effect, a proof of concept prototype of the REMS (Rover Environmental Monitoring Station) wind sensor on board the Curiosity rover has been used. The self and cross-heating effects of the thermal structures have been characterized from open-loop measurements using Diffusive Representation. These models have been proven to be suitable in the analysis of the thermal dynamics of the sensor under constant temperature operation employing the tools of Sliding Mode Controllers. This analysis allows to understand the long term heat diffusion processes in the whole structure and how they may affect the raw output signals.

*Key words:* Diffusive representation, sliding mode controllers, time-varying systems, thermal sensors

## 1. Introduction

The objective of this paper is to obtain time-varying thermal dynamics models using recent aplication of Diffusive Representation (DR), [1], of a proof of concept prototype of the REMS (Rover Environmental Monitoring Station) wind sensor. The REMS sensor suite is an instrument from the Mars Science Laboratory (MSL) on board the Curiosity rover that landed in Mars in 2012. REMS included humidity, pressure, temperature, radiation and wind velocity sensors [2, 3, 4]. In this paper, we used a prototype of the engineering model developed in 2008 that led to the flight model which is currently on board of the Curiosity rover. The prototype is very similar in concept and size to the flight model.

Wind and temperature sensors from the REMS Booms Spare Hardware have been refurbished into TWINS Booms, for NASA's Insight mission, expected to be launched in 2018 [5]. The performance in terms of dynamic range and resolution has been enhanced in these wind and temperature sensors. The same device concept, although including many significant changes in structure and number of sensors, is scheduled to fly in NASA's Mars 2020 Rover, as part of the wind sensor that will include the MEDA (Mars Environmental Dynamics Analyzer) instrument [6].

The main novelty of this paper resides in the application of diffusive representation to extract the thermal dynamical models of complex space sensor structures such as those of the wind sensors in REMS, TWINS or MEDA, which, to the best knowledge of the authors, has never been done.

*Corresponding author
*Email addresses:* maria.teresa.atienza@upc.edu (Maria-Teresa Atienza )

Figure 1: Photography of the proof of concept prototype of REMS wind sensor. One of the PCBs with a group of dice can be seen.

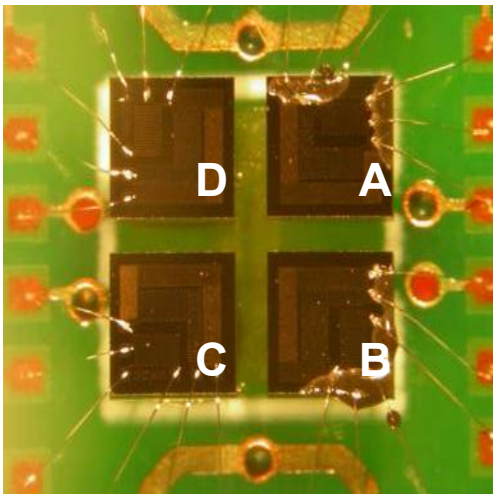


Figure 2: Photography of a dice set over the PCB. The dice are named $A$, $B$, $C$ and $D$.

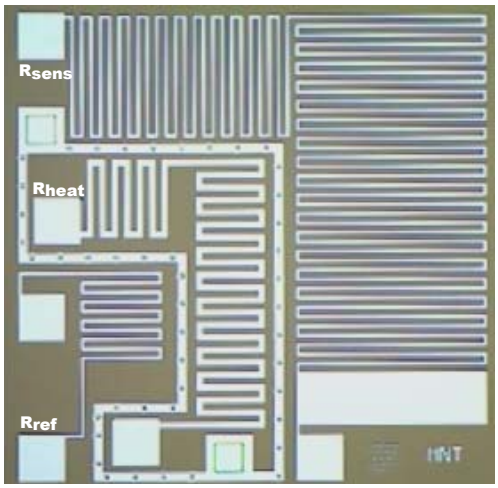


Figure 3: Zoom of one die, where the heating, sensing and reference resistors are shown. In the experiments of this paper $R_{heat}$ has been used for heating and sensing temperature.

This modeling is very important for designing the control algorithm at the system level.

All these wind sensors are based on thermal anemometry, which is the method that has been used in multiple occasions for the challenging task of sensing wind in Mars ($CO_2$ atmosphere, low pressure in the range 6-12mBar and a large temperature dynamical range from 150K to 300K) [7, 8]. It consists in the detection of the wind velocity by measuring the power dissipated of a heated element due to forced convection. The wind velocity and direction in REMS wind sensor, is detected by measuring the tangential wind components at three points of a cylindrical supporting structure (boom). This is done by measuring the convection heat transfer of four silicon dice with platinum (Pt) resistors. These resistors are grouped in sets of four in a coplanar plane, to achieve 2D wind sensitivity. Full 3D direction is measured placing three of these sets at 120° to each other in the boom. These dice-sets are placed on three PCBs (Printed Circuit Board). In Figure 1, the boom used in the experimental setup with the view of one of the resistors set on its PCB is shown. In Figure 2, one of the three silicon dice sets can be seen , while in Figure 3 the resistors' structure of one die is observed. The dice are named, $A, B, C$ and $D$. In this prototype the dice are placed on a supporting structure of Pyrex pillars to increase thermal isolation to the boom.

Diffusive Representation is a mathematical tool that allows the description of a physical phenomena based on diffusion, using state-space models of arbitrary order in the frequency domain. It is appropiate for model extraction of fractional systems, such as thermal [9, 10, 11] or electrical [12, 13, 14]. A first analysis of heat flow dynamics described by diffusive representation in a hot thin film anemometer was described in [1], where thermal models were obtained for a spherical 3D wind anemometer for different wind velocities. These models provide the temperature dynamics of the components of the system under study as a function of the power delivered to the heat sources. On the other hand, the time evolution under closed-loop operation (constant temperature control) was obtained using the theory of Sliding Mode Controllers (SMC) [15]. The necessary state-space models for the sliding mode analysis are provided from open-loop measurements at different wind velocities using Diffusive Representation modeling. These state-space models have proven to be very well suited for thermal applications [9]. In [1], each thermal dynamics model was extracted from a constant wind speed experiment. In this paper, however, the method is different, as the thermal dynamics models are extracted from a single experiment with wind velocity switching due to the working principle of the wind tunnel used. Furthermore, the obtained models are more complex, since they include self and cross-heating effects across the different subsystems in the sensor.

The REMS wind sensor is operated under constant temperature anemometry mode. This is achieved using a thermal sigma-delta modulator, which places the system within the control surface determined by *Temperature = constant* in finite time, which is followed by a sliding motion. It must be noted that in the case that concern us, the analysis of the resulting dynamics is performed under the infinite sampling frequency approximation using the tools of equivalent control typical of SMC.

The experiments described in this paper, were carried out at CAB (Center for Astrobiology, INTA-CSIC) facilities in Madrid, Spain. For the experimental setup, a five meter linear wind tunnel has been used. The wind tunnel operation mode is different from the hypobaric chamber used in [1] where a fan set the wind velocities. In this case, the tunnel has a rail inside where the sensor is positioned. The equivalent Mars velocities are achieved by moving the sensor through the rail. The sensor support also has a pan and tilt system which provides different pitch and yaw positions for the boom. Figure 4 shows the wind sensor employed in the experimental setup inside the tunnel at the start position, and with pitch and yaw angles set to 0°.

DR and SMC are used together and are explained in Section 2 of this paper. Section 3 describes the sensor and the experimental setup. Three main experimental results are shown in section 4. Firstly, in 4.1 diffusive models of the dice have been obtained for different wind conditions. Secondly, the heating of the boom due to the heating of the dice has been characterized in paragraph 4.2. The third experiment shown in subsection 4.3, consists in predicting the closed-loop behaviour from the DR models of the dice obtained previously. Finally, the conclusions of the paper are presented in section 5.

## 2. Diffusive Representation and Sliding Mode Controllers

This section describes briefly the theoretical grounds and tools of diffusive representation and sliding mode controllers used in the sensor thermal dynamics analysis.

### 2.1. Diffusive Representation

Diffusive Representation theory allows obtaining exact and approximate state realizations of a wide class of integral operators of rational or non-rational nature. Given a non-rational transfer function, $H(p)$, associated with a convolution causal operator denoted by $H(\partial_t)$, the diffusive realization of this operator is expressed by the following input ($u$) – output ($y$) state space realization of $u \longmapsto y = H(\partial_t)u = h * u$ of the form [13]:

$$\begin{array}{rcl} \frac{\partial \psi(\xi,t)}{\partial t} & = & -\xi\psi(\xi,t) + u(t), \quad \psi(\xi,0) = 0 \\ y(t) & = & \int_0^\infty \eta(\xi,t)\psi(\xi,t)d\xi \end{array} \tag{1}$$

where $\xi \in \mathbb{R}$ is frequency, $\eta(\xi,t)$ is the diffusive symbol of $H(\partial_t)$ that represents the system behaviour, i.e., how the system evolves as a function of the input signal, u(t). The state-variable $\psi(\xi,t)$ is a time-frequency representation of the input, called the diffusive representation of $u(t)$ . The diffusive symbol is a solution of the following integral equation directly obtained from Laplace transform (with respect to $t$) [13]:

$$H(j\omega) = \int_0^\infty \frac{\eta(\xi)}{j\omega + \xi} d\xi, \quad \omega \in \mathbb{R}^* \tag{2}$$

When modeling thermally a device, two distinguisable effects can be considered: the self-heating effect, due to the injection of power into the heaters of the own device, and the cross-heating effect, consequence of injecting power into heat sources in parts of the structure different from the one in which temperature is sensed. If we consider four similar devices thermally coupled, the temperature of each device when the four of them are working simultaneously will be the result of the superposition of the self and cross-heating effects. The modeling of the four coupled devices of Figure 2, $A$, $B$, $C$ and $D$, will consider four inputs ($P_A(t)$, $P_B(t)$, $P_C(t)$ and $P_D(t)$) and four outputs ($T_A(t)$, $T_B(t)$, $T_C(t)$ and $T_D(t)$). Besides, to be able to handle experimental data, a discrete approximation of $H(\partial_t)$ can be built discretizing the continuous variable $\xi$ into $\{\xi_k\}_{1\leq k\leq K}$, where $K$ is the order of the discretized model. Now equation (2) remains like this:

$$H(j\omega) = \sum_k^K \frac{\eta_k}{j\omega + \xi_k} d\xi_k, \quad \omega \in \mathbb{R}^* \tag{3}$$

from which the bandwidth of the model can be extracted from the diffusive symbol. The diffusive representation equations are the followings:

- Self-Heating. Power only in device X, the rest of the structure is passive

$$\frac{d\psi_k^X(t)}{dt} = -\xi_k\psi_k^X(t) + P_X(t), \quad \psi_k^X(0) = 0 \tag{4}$$

  where $X = A, B, C$ or $D$ is the corresponding device.

- Cross-Heating. Power only in device Y, the rest of the structure is passive

$$\frac{d\phi_j^Y(t)}{dt} = -\upsilon_j\phi_j^Y(t) + P_Y(t), \quad \phi_j^Y(0) = 0 \tag{5}$$

  for $j = 1 \ldots J$, and $Y = A, B, C$ or $D$. $J$ is the model order and $\{\upsilon_j\}$ is the discretized frequency mesh for the cross-heating models.

The frequency discretization for the self-heating effect, $\xi_k$, may be different to the frequency mesh of the cross-heating effect, $\upsilon_j$. Their model orders can also be different: $K$ for the self-heating case and $J$ for the cross-heating. In general, self and cross responses may be very different. As the frequency mesh is chosen with respect to the time response characteristics of the devices, they will be different when considering the self or the cross effects. The frequency mesh of the diffusive symbols, $\xi_k$ and $\upsilon_j$, is set according to the spectral contents of the dynamic characteristics of the system. The frequency sets are usually geometrically spaced. The minimum frequency is set to $f_{min} = U/T$, where $T$ is the total duration of the experiment and $U$ is the number of wind velocities applied during the experiment. The maximum frequency, on the other hand, is chosen accordingly with the sampling period, $f_{max} = \frac{1}{2T_s}$, where $T_s$ is the sampling period [9].

The output at each device when the four devices are working simultaneously is:

$$\begin{array}{rcl} \tilde{T}_A(t) & = & \sum_k^K \eta_k^{AA}(t)\psi_k^A(t) + \sum_j^J \eta_j^{BA}(t)\phi_j^B(t) \\ & + & \sum_j^J \eta_j^{CA}(t)\phi_j^C(t) + \sum_j^J \eta_j^{DA}(t)\phi_j^D(t) \end{array} \tag{6a}$$

$$\begin{array}{rcl} \tilde{T}_B(t) & = & \sum_j^J \eta_j^{AB}(t)\phi_j^A(t) + \sum_k^K \eta_k^{BB}(t)\psi_k^B(t) \\ & + & \sum_j^J \eta_j^{CB}(t)\phi_j^C(t) + \sum_j^J \eta_j^{DB}(t)\phi_j^D(t) \end{array} \tag{6b}$$

$$\begin{array}{rcl} \tilde{T}_C(t) & = & \sum_j^J \eta_j^{AC}(t)\phi_j^A(t) + \sum_j^J \eta_j^{BC}(t)\phi_j^B(t) \\ & + & \sum_k^K \eta_k^{CC}(t)\psi_k^C(t) + \sum_j^J \eta_j^{DC}(t)\phi_j^D(t) \end{array} \tag{6c}$$

$$\begin{array}{rcl} \tilde{T}_D(t) & = & \sum_j^J \eta_j^{AD}(t)\phi_j^A(t) + \sum_j^J \eta_j^{BD}(t)\phi_j^B(t) \\ & + & \sum_j^J \eta_j^{CD}(t)\phi_j^C(t) + \sum_k^K \eta_k^{DD}(t)\psi_k^D(t) \end{array} \tag{6d}$$

where $\eta_k^{XX} \in \mathbb{R}^K$ is the self-heating diffusive symbol for device $X$ (represents the thermal behaviour of device $X$ as a function of power injected into itself) and $\eta_j^{XY} \in \mathbb{R}^J$ is the cross-heating diffusive symbol for device $Y$ when power is being injected into device $X$ (represents the thermal behaviour of device $X$ as a function of the power injected into device $Y$).

If $\eta_k^{XX}$ is time-varying (i.e. varies with different wind velocities) the dynamical system for the self-heating case of device $X$ is described by:

$$\begin{array}{rcll} \psi_k^{X(n)}(t) & = & 0 & t \in [t_0, t_n] \\ \dot{\psi}_k^{X(n)}(t) & = & -\xi_k\psi_k^{X(n)} + u(t) & t \in [t_n, t_{n+1}] \\ \dot{\psi}_k^{X(n)}(t) & = & -\xi_k\psi_k^{X(n)} & t > t_{n+1} \end{array} \tag{7}$$

$$\tilde{T}_X(t) \quad = \quad \sum_{n,k} \eta_k^{XX(n)} \psi_k^{X(n)}(t) + \sum_k^K c_k e^{-\xi_k(t-t_0)}$$

where $\eta_k^{XX(n)} \in \mathbb{R}^K$ is the self-heating diffusive symbol of device $X$ associated to the system's conditions in the $n$-th interval in $t \in [t_n, t_{n+1}]$. $c_k \in \mathbb{R}^K$ represents the initial conditions of the system at the beginning of the measurements, at $t = t_0$. In these discretized time intervals, the diffusive symbols can be considered constant in a wind experiment. With this approach, the thermal models for different wind situations can be extracted from a single open-loop experiment, with $t \in [t_0, t_F]$, in which wind speed is continuously switched between several wind velocities. The sensor will be characterized for $U$ wind speeds, $\{w_1, \dots w_U\}$. Each wind speed is applied in an interval $t \in [t_n, t_{n+1}]_{n=0,\dots,N}$, where N is the number of wind events, such that, $N \gg U$. All the wind velocities are applied for a short time $\Delta t_n = (t_{n+1} - t_n)$, where $\Delta t_n \ll t_F$, for all $n$. In the meantime, a Pseudo Random Binary Sequence (PRBS) current is applied to the heat sources in open-loop mode with a period $T_{PRBS} \ll \Delta t_n \ll t_F$. This type of input signal has a wide frequency spectrum which improves the quality of the fittings in presence of noise [16].

The self, $\eta_k^{XX}$, and cross-heating, $\eta_j^{XY}$ diffusive symbols, together with the initial condition constants, $c_k$, are inferred by solving the finite dimensional least-squares problem formulated as in [17].

### *2.2. Sliding Mode Controllers*

It is is known that constant temperature operation mode in anemometers (CTA mode) is better in terms of time response [2]. In this operation mode, the temperature in the heating elements is forced to be constant and the power required at every element to keep constant the temperature is the output signal of the sensor. To this effect, thermal sigma-delta modulators have been used, which apply a modulated power to maintain the temperature constant in the structure, [15]. In this control, at each sampling period, $T_s$, the temperature of the hot element, $T_n = T(nT_s)$, is compared with the desired target temperature, $\Delta T$. If $T_n \geq \Delta T$, $P_{off}$ is injected into the system during the following sampling period. On the contrary, if $T_n < \Delta T$, $P_{on}$ is injected. In the literature other control methods can be encountered to maintain the temperature constant in a thermal sensor, as in [18] and [19]. In this paper, the analysis of the closed-loop dynamics has been undertaken using the tools of equivalent control, typical of sliding mode controllers for the infinite sampling frequency approximation. These types of controllers alter the dynamics of the system by applying a discontinuous control signal so that under some conditions the system 'slides' on a certain control surface [1, 15]. For the general case of finite order thermal systems, the following control surface is defined:

$$\sigma(\psi(t)) = \Delta T - \tilde{T}_X(t) = \Delta T - \sum_{n,k} \eta_k^{XX(n)} \psi_k^{X(n)}(t) \quad (8)$$

where $\tilde{T}_X(t)$ is the temperature in device $X$. If the reachability conditions from [1] are accomplished, the system will be placed within the control surface $\sigma(\psi(t)) = 0$ in finite time.

The equivalent control under a sliding motion that maintains the temperature of the thermal structure constant is given by the condition $\dot{\sigma}(\psi(t)) = 0$. For a system described by diffusive representation the equivalent control is [1]:

$$u_{eq}(t) = \Gamma^{(n)-1} \sum_{m,k} \eta_k^{XX(m)} \xi_k \psi_k^{X(m)}(t) \quad t \in [t_n, t_{n+1}] \quad (9)$$

where $\Gamma^{(n)} = \sum_k \eta_k^{XX(n)}$. In [1] and [17], a more complete development of SMC theroy can be found.

The time evolution of the power requiered to maintain the temperature constant can be predicted by the SMC analysis, even in the case of wind speed changes. The equivalent control is predicted from the diffusive symbols for each specific wind velocity inferred in the open-loop characterization. In the closed-loop experiment, the wind is kept constant within the time intervals $\Delta t_n = (t_{n+1} - t_n)$, for $n = 0, \dots N$, where $N$ is the number of wind intervals such as $N \geq U$, in this case.

## 3. Experimental Setup Description

In this section, a detailed description of the sensor and of the wind tunnel used in the experiments is given. As it has been mentioned above, for the experimental measurements the wind sensor was enclosed in a five meter linear wind tunnel. The air pressure inside the tunnel was set to 240 mBar and the experiments were made at room temperature. Air temperature and pressure information

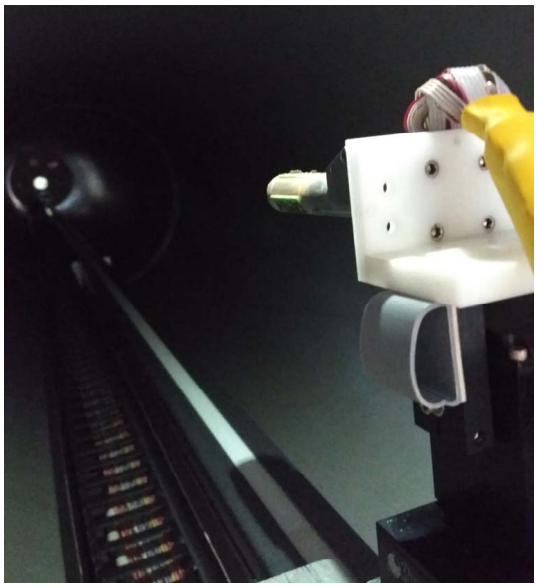

Figure 4: Photography of the prototype of REMS wind sensor inside the tunnel used in the experiments. In this photo, the sensor is positioned at the start position (0m) with pitch and yaw angles set to 0°.

is provided by four temperature and four pressure sensors placed along the tunnel. The operating method of the tunnel consists of a car on a rail that moves at a certain velocity. The range of velocities the car can take goes from 6m/min to 30m/min. At the given pressure and temperature conditions, the equivalent Mars wind velocities that provide the same Reynolds numbers range approximately from 2m/s to 10m/s. The tunnel has a pan and tilt system that allows the boom to move in yaw direction $\pm 165°$ and in pitch direction $+33°$ and $-43°$. Depending on the pitch and yaw position of the boom, the signal observed at a given velocity will be different in forward movements (from 0m to 5m position) than in reverse movements (from 5m to 0m position). The time the car lasts in travelling from the start to the finish position points ranges from 50s to 10s (for 6m/min and 30m/min respectively), which is a very short time taking into account the expected values of some time constants in the system.

The prototype of the REMS wind sensor is composed of three PCBs placed on a cilyndrical boom of 152mm lenght and 20mm diameter. Inside the boom, a Pt100 resistor measures its temperature. The three PCBs are 120° from each other with four silicon dice set in each one. The dice of each set have a dimension of 1.5x1.5 mm and are named: $A$, $B$, $C$ and $D$, and they are positioned as a grid (see Figure 2). Each die contains three platinum resistors, one for heating, another for temperature sensing and a third one used as a temperature reference within the closed loop (see [2]). These resistors can be observed in Figure 3. The electrical conexion between the PCB and the resistors is made by a wire bonding process. The resistors were fabricated in clean room facilities using a silicon wafer. Silicon oxide ($SiO_2$) was grown thermally for electrical isolation. On top of the $SiO_2$, the platinum resistors were patterned with a photolitography process. The platinum, thanks to its high temperature coefficient of resistance, is the most suitable material for these devices [20]. In our case, only the heating resistor has been used, both for heating and measuring the temperature. The dice's heating resistors are named $R_A$, $R_B$, $R_C$ and $R_D$, and their nominal resistance values at 0°C are: $R_{0A} = 1767\Omega$, $R_{0B} = 1753\Omega$, $R_{0C} = 1755$, and $R_{0D} = 1760\Omega$. The resistors of the PCB on the top of the boom, when this is placed parallel respect the longitudinal axis of the tunnel, have been used in the measurements.

For the measurements, a National Instruments' FPGA connected to a PC and located outside the tunnel is used. Both the open and closed-loop operation modes of the experiments are implemented in the FPGA.

## 4. Experimental Results

In this section the experimental results obtained from the application of the theory described in section 2 are explained. Three main experimental results have been obtained. Firstly, in experiments $A.1$ to $A.4$, the thermal dynamics models of self-heating and cross-heating of the silicon dice, at different wind velocities, have been obtained. From the obtained models, the prediction of the temperature of each dice when all the resistors are working together has been made. Secondly, from experiment $B.1$, a DR model has been obtained describing the temperature evolution in the boom as a result of the total power injected in the four dice of one PCB. Finally, the prediction of the output power of the sigma-delta modulator of a die working in closed-loop under constant temperature mode has been made in experiment $C.1$.

### *4.1. Thermal dynamics model of self-heating and cross-heating of the silicon dice at different wind velocities*

The self-heating models have been obtained for two cases, for wind velocity zero (no movement of the car) and for Mars equivalent wind velocity $\pm 2.5$m/s.

For the zero wind velocity case (experiment $A.1$), four identical experiments have been carried out. Each experiment consisted in exciting only one of the Pt resistors of the dice set ($R_A$, $R_B$, $R_C$ or $R_D$) with a 10Hz PRBS of current, between 1mA and 4mA, while the rest of the resistors of

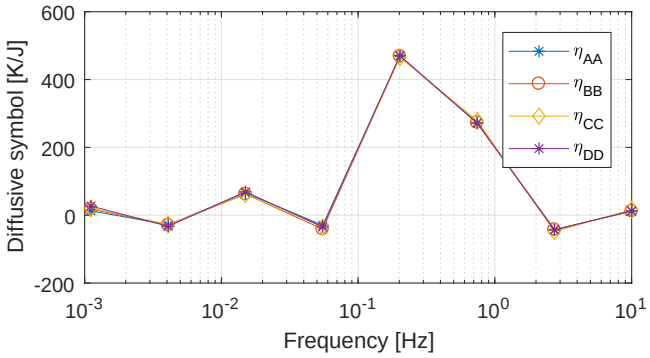


Figure 5: 8-th order self-heating diffusive symbols of each die ($A$, $B$, $C$ and $D$) at zero wind velocity, obtained from experiment $A.1$. The four diffusive symbols are very similar among them.

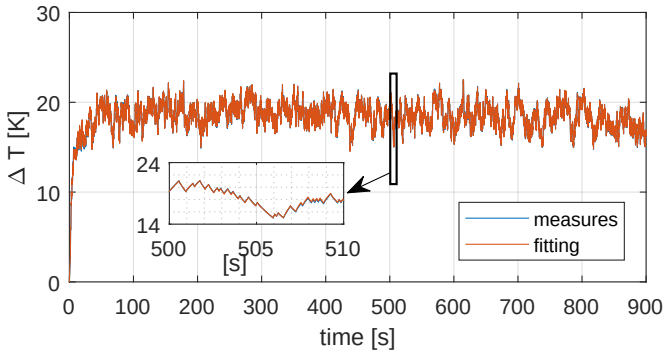


Figure 6: Fitting of time evolution of the temperature of die $B$ at zero wind velocity from the open-loop experiment $A.1$. There is a good agreement between the experimental data (in blue) and the fitting data (in red). The inset figure shows a 10s zoom.

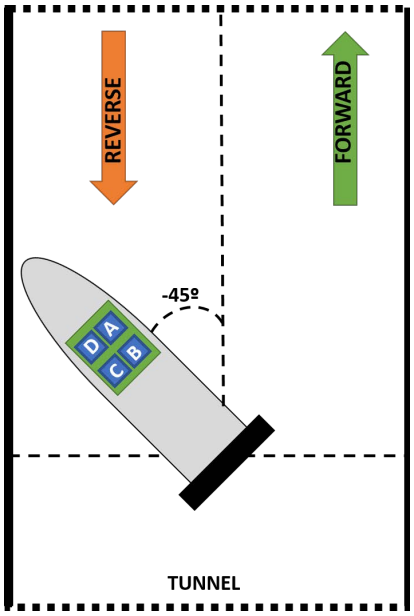


Figure 7: Top view of the boom inside the tunnel. Boom is positioned at pitch 0°, yaw −45° to ensure good sensitivity in die B both in forward and reverse movements.

the sensor system are switched off. Each experiment lasted 15 minutes and it was sampled with a period $T_s = 0.05$s. Taking these parameters into account the frequency mesh for the diffusive model is set in the range $\{1.1\text{x}10^{-3}, 10\}$Hz while the model order chosen is set to $K = 8$. In Figure 5 the diffusive symbols obtained for the four dice ($A$, $B$,$C$ and $D$) are shown. The four diffusive symbols for each die are almost indistinguishable among them. This is something to be expected since the four components have the same thermal characteristics. A frequency peak can be encountered around 0.2Hz. As the fitting is done with an arbitrary discretization of the frequency, the frequency set with significant values of the diffusive symbols give an approximate value of the time constants of the thermal filters of the system. To avoid repetition, only the fitting of the experimental measurement of die $B$ is shown in Figure 6. As it can be observed in the zoom of the Figure 6, the matching between experimental and fitting data is good.

In the case of Mars equivalent wind velocities ±2.5m/s (experiment $A.2$), only die $B$ has been analyzed. For this experiment, the pan and tilt system is set to pitch angle 0° and yaw angle −45°. This choice in the boom position is made based on the best wind incidence in die $B$ when the car is moving. At this position, a good wind sensitivity, both in forward and reverse movements, is ensured in die $B$ (see Figure 7). The experiment consisted in a continuous sequence of forward and reverse movements of the car, therefore, good sensitivity in both directions was needed to obtain the models for the two velocities given:

- for $v = +2.5$m/s from 0m to 5m.
- for $v = -2.5$m/s from 5m to 0m.

It must be noted that, although die $B$ has good sensitivity to both movements, the response is higher in the forward direction. If we look at the top view of the boom of Figure 7, it can be observed that in forward movements dice $A$ and $B$ are the two most sensitive to the wind. However, in reverse movements, die $B$ is left behind respect dice $C$ and $D$ and therefore its response is not as high.

During experiment $A.2$, a 20Hz PRBS sequence of current, between 1mA and 4mA, was injected in the heater of die $B$, while the rest of the resistors remained off. The experiment lasted 1700s, and the sampling frequency was set to 40Hz. The geometrically distributed frequency mesh is set in the range $\{1.7\text{x}10^{-3}, 20\}$Hz and the model order

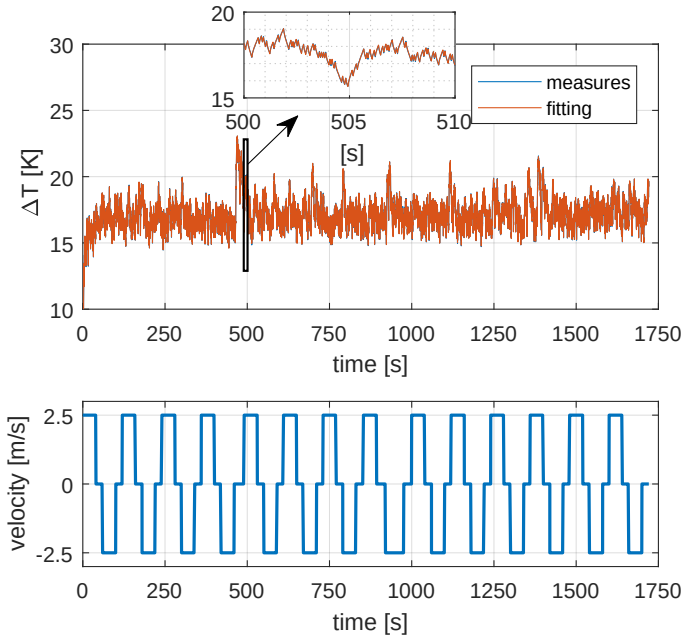


Figure 8: Top: Fitting of the time evolution of the temperature of die $B$ with velocities ±2.5m/s, from open-loop experiment $A.2$. In blue, the experimental data, and in red the fitting data is shown. The inner figure shows a 10s zoom. Bottom: Wind velocity sequence applied to the die along experiment $A.2$.

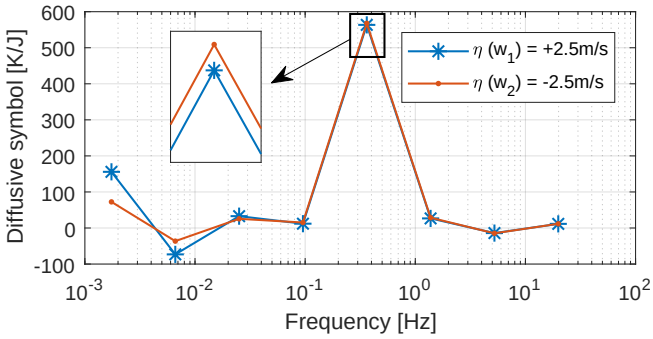


Figure 9: 8-th order self-heating diffusive symbols for die $B$ for velocities ±2.5m/s, obtained from experiment $A.2$. There is a frequency peak at approximately 0.3Hz, where diffusive symbols are distinguisable between each other.

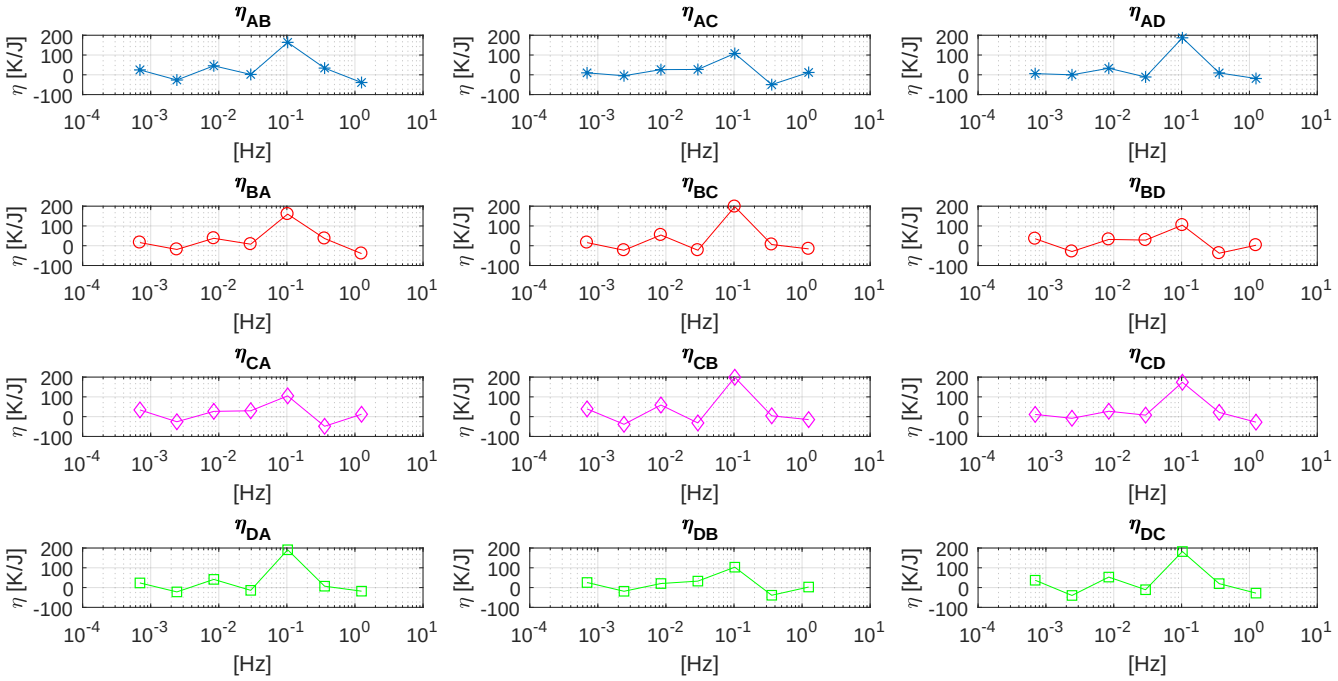


Figure 10: Cross-Heating diffusive symbols for dice $A$, $B$, $C$ and $D$, inferred from experiment $A.3$. The active die in the first row (all in blue) is $A$. In the second row (all in red) the active die is $B$. In the third row (all in pink) the active die is $C$. And finally, in the fourth row (all in green) the active die is $D$. The nine cross-heating diffusive symbols have an order $J = 7$, and their frequency peak is around 0.1Hz.

chosen is set again to $K = 8$. Figure 8 shows the fitting of the temperature measurement together with the wind velocities applied inside the tunnel. There is a good agreement between experimental and fitting data. Besides, Figure 9 shows the obtained diffusive symbols for $v = \pm 2.5$m/s. As observed, the diffusive symbols are distinguishable from each other, depending on their wind velocity, in the unique frequency peak at approximately 0.3Hz. The wind dependence can be parameterized as a variable amplitude of the pole at that frequency. At higher wind speeds, the temperature in the die is lower which means that the amplitude in the corresponding diffusive symbol is lower too. In [17], the relationship between different wind velocities and amplitudes can be observed better for a spherical wind sensor using the same sensing principles.

On the other hand, the DR cross-heating models have been obtained (experiment $A.3$). In this case, the temperature evolution of a die is obtained from the heat dissipated in another die where power is being injected. It has been observed empirically that in presence of different wind velocities, no sustainable differences are observed in the cross-heating diffusive symbols, therefore, only the zero wind velocity case is presented.

In experiment $A.3$, four identical measurements have been carried out to obtain each die's cross-heating diffusive symbols. The die where the PRBS current sequence is injected is considered the *active* die. In each measurement, a 1.25Hz PRBS current between 1mA and 4mA is injected in the *active* die of a PCB, while the remaining dice of the PCB are measured with a low current to avoid self-heating. The four experiments lasted 1 hour and were sampled at a 2.5Hz frequency. The frequency mesh for all is approximately in the range $\{2.7\text{x}10^{-4}, 0.2\}$Hz, and the order chosen for the cross models is $J = 7$. As the cross-heating effect is expected to have a slower respone, the excitation PRBS current is of a lower frequency than the used when obtaining the self-heating models. Figure 10 shows the cross-heating diffusive symbols obtained from the experiments. At each row, the diffusive symbol for each die respect to the active die is observed. For example, the first row represents the diffusive symbols of dice $B$, $C$ and $D$ when the active die is $A$. The models are symmetric with respect to the active die. The thermal influence of the adjacent dice to the active die is always similar, whereas the die in diagonal respect to the active one is heated differently and with much smaller amplitude. For example, if we look at the first row of Figure 10 the diffusive symbols, $\eta_{AB}$ and $\eta_{AD}$ are very similar between them, as dice $B$ and $D$ are adjacent to the the active die $A$. Similarly, in the second row we can see the similitude between diffusive symbols $\eta_{BA}$ and $\eta_{BC}$, because $A$ and $C$ are adjacent to active die $B$ in this case. At the same time, the four mentioned diffusive symbols take the same shape. In the same way, this concordance also happens with the diagonally positioned die. The most significant frequency peak in the cross-heating models is around 0.1 Hz. In these models a displacement of the frequency peak to lower frequencies can be observed, due to the slow dynamics of

the cross-heating if comparing with the self-heating models. This cross-heating is due to thermal transport within the boundary layer and thermal conduction through the set pillars–PCB.

From the models of Figures 5 and 10, from experiments $A.1$ and $A.3$, it is possible to predict the temperature at each die when all the dice are working simultaneously, applying superposition as in equation (6). The DR models have been validitaded in the four dice at zero wind speed. Results from die $B$ are only presented due to the similarity among the other dice's predictions. In this experiment, $A.4$, of 1h of duration, a 10Hz PRBS sequence between 1mA and 4mA is injected in the four dice, while the temperature at each die is registered with a sampling period of 0.05s. The input signal is fed into the self and cross-heating models and by superposition the temperature prediction is obtained. Figure 11 shows the experimental temperature evolution of die $B$ and the predicted temperature from the models. In Figure 12 the self-heating and cross-heating independent temperature contributions, together with die $B$'s temperature measurement is shown. As it can be observed, the total temperature of the die, depends on how much the die has been heated by its own injection of power (self-heating) and by the heating produced by the rest of the dice (cross-heating).

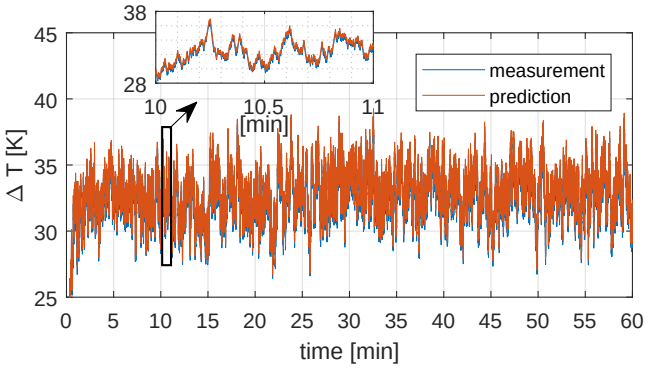


Figure 11: Prediction of the open-loop temperature evolution of die $B$ when all the dice are working simultaneously, in experiment $A.4$. There is good matching between the experimental measurement (in blue) and the superposition of the models output (in red) as shown in the zoom of 1min of the inner figure.

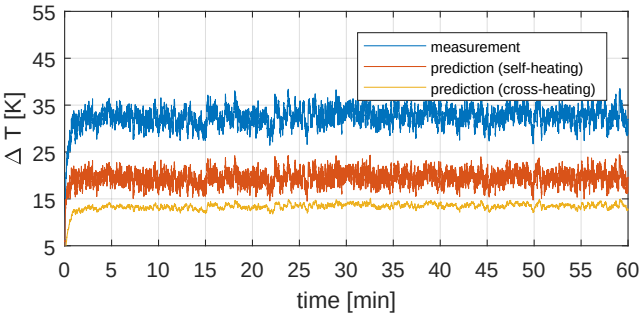


Figure 12: In blue the experimental measurement of the temperature of die $B$, when all the dice are working simultaneously in experiment $A.4$ is shown. The contribution of the self-heating effect (in red) and of the cross-heating effect (in yellow) are shown independently.

### *4.2. Boom heating DR model*

The objective of this subsection is to model the heating of the boom as a result of the power injected in the dice. To this effect, a diffusive representation thermal model of the boom has been obtained. For this task, one of the sensor's PCB is made to work under constant temperature mode. The sum of the necessary power to maintain constant the temperature in all the dice is going to be the input of the DR system. Therefore, to provide variability to the input signal, as no wind velocity was applied, the target temperature set on the dice was changed randomly every 5 minutes among three different constant values: 315K, 320K and 325K. Experiment $B.1$ lasted 20h and was sampled every 0.1s. The sigma-delta current in the four dice was set to $I_{low} = 1$mA and $I_{high} = 4$mA. As mentioned before, the input of the DR system is the sum of the dissipated power of all the dice, while the output of the model is the difference between the temperature of the boom and the air temperature. Specifically we have:

$$\begin{aligned} u(t) &= P_A(t) + P_B(t) + P_C(t) + P_D(t) \\ y(t) &= \Delta T = T_{boom}(t) - T_{amb}(t) \end{aligned} \qquad (10)$$

where $T_{amb}(t)$ is the air temperature inside the tunnel and $T_{boom}$ is the boom temperature. Air temperature is obtained from the sensors along the tunnel. The model order chosen in this case is $J = 6$. In Figure 13, the evolution of the changing temperature of the four dice along the whole experiment is shown. On the other hand, on top of Figure 14, the fitting of the difference between the boom and the air temperature is observed, where there is a reasonable matching between the experimental measurements and the fitted data. Below, the inferred 6-th order diffusive symbol is presented. It has a maximum between $f = 2\text{x}10^{-4}$Hz and $f = 2\text{x}10^{-3}$Hz. These low values make sense since the heating of the boom was expected to be slow. Furthermore, it follows that the boom structure is thermally coupled to the dice and therefore the heating of the boom may generate drifts in the sigma-delta power dissipated on the dice when the sensor is under regular operation. This will be further disccused in subsection 4.4.

### *4.3. Prediction of the closed loop output from self-heating model*

Finally, the prediction of the closed-loop dynamics is going to be obtained using SMC theory when different wind velocities are being applied. Again, the boom is positioned at pitch 0° yaw −45° angles and die $B$ is chosen for this experiment, numbered $C.1$. The wind velocities for the experiment are the ones characterized in section 4.1,

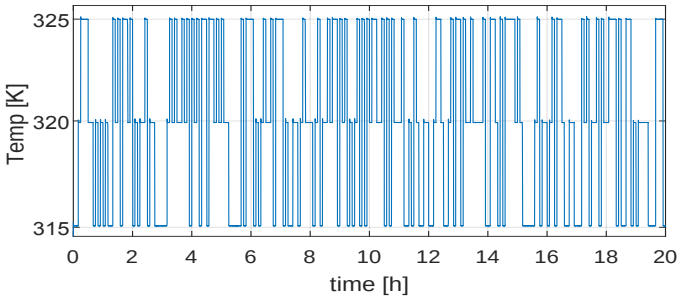


Figure 13: Temperature evolution of dice $A$, $B$, $C$ and $D$ along experiment $B.1$. The target temperature changed every 5min among three values: 315K, 320K and 325K.

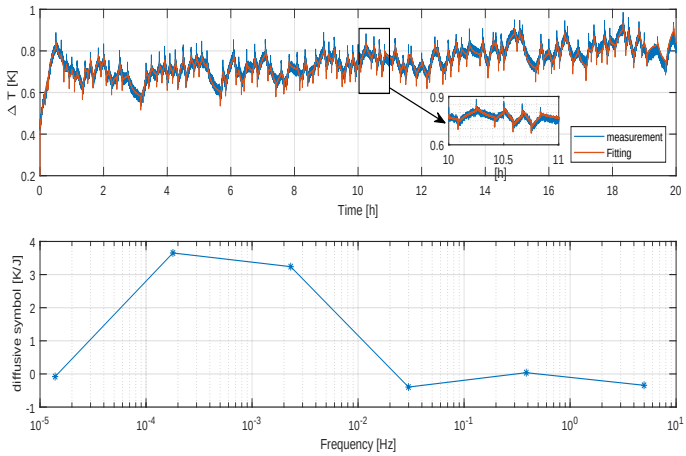


Figure 14: Experimental data (in blue) Vs fitting data (in red) along the 20h of experiment $B.1$, where the temperature of the dice has been changing randomly every 5min. Bottom: 6-th order diffusive symbol of the boom.

$v = \pm 2.5$m/s ($A.2$) and $v = 0$m/s ($A.1$). In $C.1$ experiment, die $B$ was maintaned at a constant target temperature $\Delta T = 17.2$K while the rest of the dice were switched off and the wind sequence of Figure 15 (below) was applied for approximately 290s. From the DR models for each wind velocity (those of Figures 5 and 9), the prediction of the necessary power to maintain the temperature constant has been done. In the top of Figure 15, the predicted equivalent control together with the experimental control waveform can be observed, with a good agreement between both. As it is observed, the diffusive approach presented in this paper, allows to predict the thermal dynamics of a wind sensor under wind switching conditions.

### *4.4. Discussion*

As it has been seen in sections 4.1 and 4.2, cross-heating effects are present in the sensor structure, both in the dice and in the boom. These effects, specially the heating of the boom, can introduce drifts in the average power of the dice under normal operation. In order to avoid these undiserable effects in the REMS wind sensor, differential

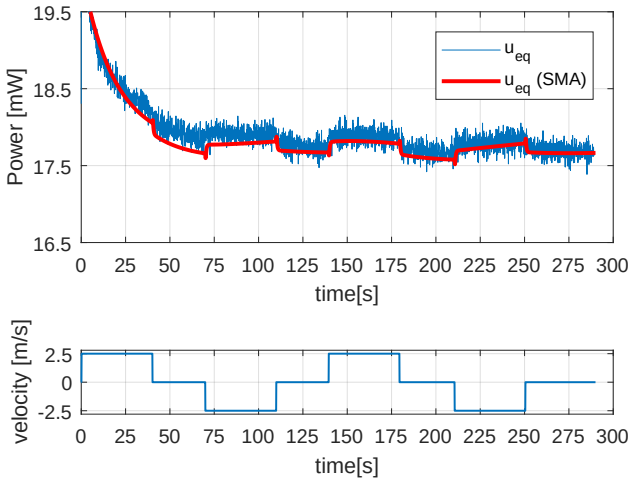


Figure 15: Top: Experimental average power injected into the heater of die $B$ under closed loop control (in blue) and the the result of applying the sliding mode analysis using the diffusive symbols of Figures 5 and 9 (in red). Bottom: Sequence of the wind velocities along the experiment $C.1$.

estimators in the wind retrieval algorithm were designed. The four dice $A$, $B$, $C$ and $D$ were grouped according to a North-South and East-West convection, $D$ and $A$ belonging to the North of the PCB and with $C$ and $B$ belonging to the South. Similarly, $D$ and $C$ belong to East, and $A$ and $B$ belong to the West. (See [2] for more details). The output power of each dice was computed with two differential magnitudes, cancelling any drift produced, as:

$$\begin{aligned} North - South = & \quad (P_A + P_D) - (P_B + P_C) \\ East - West = & \quad (P_C + P_D) - (P_A + P_B) \end{aligned}$$

Thus, it is to be expected that the influence of the long term temperature drifts will be cancelled when using these estimators. The corroboration of this cancellation may be an interesting future work for this type of sensors.

## 5. Conclusions

A proof of concept prototype of the REMS wind sensor, based on anemometry, has been thermally characterized in this paper. From open-loop measurements, DR thermal models of different parts of the sensor structure have been obtained for different wind velocities, differentiating between the self-heating and the cross-heating effects. Furthermore, the diffusive state-space models obtained have been proven to be well suited for predicting the close-loop behaviour of the sensor under constant temperature operation mode using the theory of SMC. The obtained models help to understand the long term effects in the temperature due to the thermal coupling of the sensor's components.

## Acknowledgments

The authors wish to thank to the Instrumentation Department of Center for Astrobiology their support during this work, specially to J. Torres, S. Carretero, S. Navarro, M. Marín and J. Gómez-Elvira.

## Funding

This work was supported in part by the Spanish Ministry MINECO under Projects ESP2016-79612-C3-2-R and FPI grant BES-2012-057618.

## References

[1] M. Dominguez-Pumar, M. T. Atienza, L. Kowalski, S. Novio, S. Gorreta, V. Jimenez, S. Silvestre, Heat flow dynamics in thermal systems described by diffusive representation, IEEE Transactions on Industrial Electronics PP (99) (2016) 1–1. doi:10.1109/TIE.2016.2605621.

[2] M. Domínguez, V. Jiménez, J. Ricart, L. Kowalski, J. Torres, S. Navarro, J. Romeral, L. Castañer, A hot film anemometer for the martian atmosphere, Planetary and Space Science 56 (8) (2008) 1169 – 1179. doi:http://doi.org/10.1016/j.pss.2008.02.013.

[3] J. Gómez-Elvira, C. Armiens, L. Castañer, M. Domínguez, M. Genzer, F. Gómez, R. Haberle, A.-M. Harri, V. Jiménez, H. Kahanpää, L. Kowalski, A. Lepinette, J. Martín, J. Martínez-Frías, I. McEwan, L. Mora, J. Moreno, S. Navarro, M. A. de Pablo, V. Peinado, A. Peña, J. Polkko, M. Ramos, N. O Renno, J. Ricart, M. Richardson, J. Rodríguez-Manfredi, J. Romeral, E. Sebastián, J. Serrano, M. de la Torre Juárez, J. Torres, F. Torrero, R. Urquí, L. Vázquez, T. Velasco, J. Verdasca, M.-P. Zorzano, J. Martín-Torres, Rems: The environmental sensor suite for the mars science laboratory rover, Space Science Reviews 170 (1) (2012) 583–640. doi:10.1007/s11214-012-9921-1.

[4] S. Rafkin, J. Pla-Garcia, C. Newman, V. Hamilton, J. Martin-Torres, M. PazZorzano, H. Kahanpaa, E. Sebastian, The meteorology of gale crater determined from msl rems data and mesoscale modeling, in: Proc. 8th Int. Conf. Mars, 2014, pp. 1–2.

[5] T. Velasco, J. A. Rodríguez-Manfredi, The TWINS Instrument On Board Mars Insight Mission, in: EGU General Assembly Conference Abstracts, Vol. 17 of EGU General Assembly Conference Abstracts, 2015, p. 2571.

[6] L. Tamppari, J. A. Rodriguez-Manfredi, M. de la Torre-Juárez, N. Bridges, P. G. Conrad, M. Genzer, F. Gomez, J. Gomez-Elvira, A. M. Harri, M. T. Lemmon, G. Martinez, S. Navarro, C. E. Newman, S. Perez-Hoyos, O. Prieto, M. Ramos, A. Saiz-Lopez, A. Sanchez-Lavega, J. T. Schofield, M. D. Smith, The Mars Environmental Dynamics Analyzer (MEDA): A Suite of Environmental Sensors for the Mars 2020 Rover, AGU Fall Meeting Abstracts.

[7] L. Gottesdiener, Hot wire anemometry in rarefied gas flow, Journal of Physics E: Scientific Instruments 13 (9) (1980) 908.

[8] C. Holstein-Rathlou, J. Merrison, J. J. Iversen, A. B. Jakobsen, R. Nicolajsen, P. NÃ¸rnberg, K. Rasmussen, A. Merlone, G. Lopardo, T. Hudson, D. Banfield, G. Portyankina, An environmental wind tunnel facility for testing meteorological sensor systems, Journal of Atmospheric and Oceanic Technology 31 (2) (2014) 447–457. doi:10.1175/JTECH-D-13-00141.1.

[9] B. Allard, X. Jorda, P. Bidan, A. Rumeau, H. Morel, X. Perpina, M. Vellvehi, S. M'Rad, Reduced-Order Thermal Behavioral Model Based on Diffusive Representation, Power Electron. IEEE Trans. 24 (12) (2009) 2833–2846. doi:10.1109/TPEL.2009.2028231.

[10] S. M'Rad, B. Allard, H. Morel, A. Ammous, N. Masmoudi, Analytic thermal modelling of power electronic components: The diffusive representation, in: Integrated Power Systems (CIPS), 2006 4th International Conference on, 2006, pp. 1–6.

[11] S. Mrad, P. Lefranc, P. Dessante, P. Chiozzi, G. Blondel, M. Fakes, P. Masson, A compact transient electrothermal model for integrated power systems: Automotive application, in: 2009 35th Annual Conference of IEEE Industrial Electronics, 2009, pp. 3755–3760. doi:10.1109/IECON.2009.5415127.

[12] C. Restrepo, G. Garcia, J. Calvente, R. Giral, L. MartÃnez-Salamero, Static and dynamic current-voltage modeling of a proton exchange membrane fuel cell using an input-output diffusive approach, IEEE Transactions on Industrial Electronics 63 (2) (2016) 1003–1015. doi:10.1109/TIE.2015.2480383.

[13] L. Laudebat, P. Bidan, G. Montseny, Modeling and optimal identification of pseudodifferential electrical dynamics by means of diffusive representation-part i: modeling, Circuits and Systems I: Regular Papers, IEEE Trans. 51 (9) (2004) 1801–1813. doi:10.1109/TCSI.2004.834501.

[14] M. T. Atienza, S. Gorreta, J. Pons-Nin, M. Dominguez-Pumar, Characterization of dielectric charging in mems using diffusive representation, IEEE Transactions on Industrial Electronics PP (99) (2016) 1–1. doi:10.1109/TIE.2016.2612619.

[15] H. Sira-RamÃrez, Sliding Mode Control. The Delta-Sigma Modulation Approach, Birkhauser Basel, 2015.

[16] J. Davidson, D. Stone, M. Foster, D. Gladwin, Improved Bandwidth and Noise Resilience in Thermal Impedance Spectroscopy by Mixing PRBS Signals, Power Electron. IEEE Trans. 29 (9) (2014) 4817–4828. doi:10.1109/TPEL.2013.2288936.

[17] M.-T. Atienza, L. Kowalski, S. Gorreta, V. Jiménez, L. M. Castañer, M. Domńguez-Pumar, Sliding mode analysis applied to improve the dynamical response of a spherical 3d wind sensor for mars atmosphere, Sensors and Actuators A: Physical 267 (Supplement C) (2017) 342 – 350. doi:https://doi.org/10.1016/j.sna.2017.09.044.

[18] K. Toda, I. Sanemasa, K. Ishikawa, Simple temperature compensation of thermal air-flow sensor, Sensors and Actuators A: Physical 57 (3) (1996) 197 – 201. doi:https://doi.org/10.1016/S0924-4247(97)80114-8.

[19] V. Stornelli, G. Ferri, A. Leoni, L. Pantoli, The assessment of wind conditions by means of hot wire sensors and a modifed wheatstone bridge architecture, Sensors and Actuators A: Physical 262 (Supplement C) (2017) 130 – 139. doi:https://doi.org/10.1016/j.sna.2017.05.005.

[20] F. Mailly, A. Giani, R. Bonnot, P. Temple-Boyer, F. Pascal-Delannoy, A. Foucaran, A. Boyer, Anemometer with hot platinum thin film, Sensors and Actuators A: Physical 94 (1) (2001) 32 – 38. doi:https://doi.org/10.1016/S0924-4247(01)00668-9.

## Biographies

**Maria-Teresa Atienza** received the B.Sc. degree in Electronic Engineering and the M. Sc. degree in Physics Engineering from the Basque Country University, Spain, in 2012 and 2013 respectively. She joined Micro and Nano Technologies Research Group of the Universitat Politécnica de Catalunya (UPC), Spain, as a Ph.D. degree student where she is working on the identification of thermal systems applied to wind sensors for space applications.

**Lukasz Kowalski** obtained MSc degree in Electronics and Telecommunications from the Technical University of Lodz, Poland in 2005. He obtained PhD from Universitat Politécnica de Catalunya, Spain in 2016 for thesis 'Contribution to advanced hot wire wind sensing'. He has joined MNT group in September 2005. He has participated in space exploration projects: REMS(MSL), MEIGA (MetNet), MEDA (Mars2020). His work is aimed to the development of thermal anemometers for the atmosphere of Mars. His research areas include dimensionless analysis, FEM/CFD simulations, thermal modeling, inverse algorithm optimization for wind speed and incidence angle retrieval. He has co-authored two patents and several scientific papers.

**Sergi Gorreta** received the M.Sc. degree in Telecomunication Engineering and the M.Sc. degree in Electronic Engineering from the Universitat Politècnica de Catalunya (UPC), Spain, in 2010 and 2011 respectively. He is currently with the Micro and Nano Technologies Research Group of the UPC as a Ph.D degree student. His working areas are sensors for space applications, integrated circuit design, non linear circuits for MEMS and control of dielectric charging in MEMS switches.

**Vicente Jiménez** received the M.Sc. degree in 1992 and the Ph, degree in 1997 from the Universitat Politécnica de Catalunya (UPC), Barcelona, Spain. He has been with the Electronic Engineering Department, UPC, since 1992, when he became Associate Professor. His research areas include digital BiCMOS design, development of microsystem circuit interfaces, and microsystem modelling. He has participated in industry and space projects related to liquid and gas thermal flowmeters. He has coauthored more than 20 scientific papers in international journals and conferences.

**Manuel Domínguez-Pumar** received the M.Sc. and Ph.D. degrees in electronic engineering from the Universitat Politécnica de Catalunya (UPC), Barcelona, Spain, and the M.Sc. (Hons.) degree in mathematics from the Universidad Nacional de Educación a Distancia, Madrid, Spain, in 1994, 1997, and 2005, respectively. Since 1994, he has been with the Department of Electronic Engineering, UPC, where he is currently an Associate Professor. From September 2006 to August 2007, he was a Visiting Scholar at the Courant Institute of Mathematical Sciences, New York, NY, USA.He is participating in the design of the MEDA wind sensor for NASA Rover2020. His research interests include control theory, chemical sensors, MEMS/NEMS sensors and actuators, dielectric charge control, sensors for space applications, sigma-delta modulation, and dynamical systems in general. Dr. Domínguez-Pumar received the 2013 NASA Group Achievement Award as a member of the Mars Science Laboratory REMS Instrument Development Team.